Research Article

Ayman H. Ahmed*

N,*N*′-Bis[2-hydroxynaphthylidene]/[2-methoxybenzylidene] amino]oxamides and their divalent manganese complexes: Isolation, spectral characterization, morphology, antibacterial and cytotoxicity against leukemia cells

https://doi.org/10.1515/chem-2020-0044
received September 11, 2019; accepted February 18, 2020

Abstract: Manganese(II) complexes of oxalic dihydrazones {*N*,*N*′-bis[2-hydroxynaphthylidene]amino]oxamide (BHO) and *N*,*N*′-bis[2-methoxybenzylidene]amino]oxamide (BMO)} have been synthesized by a general methodology. Hydrazone ligands (BHO and BMO) were obtained by the condensation of oxalic dihydrazide with 2-hydroxynaphthalene-1-carbaldehyde and 2-methoxybenzaldehyde. From the data obtained from the spectral (mass, IR, ^{1}H-NMR, UV-Vis, ESR), magnetic and thermal measurements in addition to the elemental analyses (CHNM), the structures of ligands and their complexes have been determined. The scanning electron microscope (SEM) was used to characterize the morphology of the complex surface. The ligands coordinated with the metal center in a bi-dentate way forming binuclear Mn–BHO and mononuclear Mn–BMO complexes. The manganese complexes are proposed to have octahedral stereochemistry. The ligands and manganese(II) complexes have been assessed for their antibacterial and antileukemia activities. The proliferation hindrance for the free ligands was enhanced upon coordination with the manganese(II) ions.

Keyword: hydrazone complexes, structure elucidation, pharmacological application

1 Introduction

Choosing ligands is very significant in determining the properties of coordination compounds. A ligand framework having electronegative atoms like N and O improves the coordination outcomes. Among nitrogen–oxygen giver ligands, hydrazones have an extraordinary spot because of broad applications for medication plans, insecticides and organocatalysis [1–3]. Hydrazones that are recently recognized as polyfunctional ligands have a high tendency to form stable metal complexes with d-block elements like Mn(II) due to its complexing ability through keto–enol tautomerism and availability of donor sites [4]. Although many hydrazone complexes of transition metals [M = Co^{II}, Ni^{II}, Cu^{II}, Mn^{II}, Pd^{II}, Ru^{II} and V^{IV}] are being investigated [5,6], only very few papers on aryl oxalic dihydrazone complexes were published [7,8]. This may be due to the weak dissolvability of oxalic dihydrazone ligands in commonly used organic solvents. The oxalic dihydrazones (BHO and BMO) are just soluble in highly polar solvents, for example, dimethylsuphoxide (DMSO) and dimethylformamide (DMF), while insoluble in water and other common organic solvents. Obviously, this requires great effort to refine and separate their chelates. Some complexes of *N*,*N*′-bis[2-hydroxynaphthylidene]/[2-methoxybenzylidene] amino]oxamides with Cu(II), Ni(II) and Pd(II) have been reported elsewhere [8–10], and this study is an expansion of the past work. In terms of biological activity, hydrazones including oxalic dihydrazone and their complexes offer a wide scope of pharmacological applications as antitumoral, antiviral and antimicrobial agents [8,11–13]. Metal complexes obtained from arylhydrazones are helpful in the pharmaceutical field [14] and act as enzyme inhibitors. As hydrazones having an azomethine proton (–CH=N–) establish a significant class of compounds that may be used to develop a new drug, numerous researchers have tested their biological activities. Broad investigations have uncovered that the lone pair on the azomethine nitrogen in hydrazones is liable for their chemical and biological activities [14,15]. Throughout the years, a large number of organic/inorganic compounds have been prepared to battle pathogenic microorganisms. In this regard, the Ni(II), Co(II) and Fe(III) complexes of some drugs, e.g., chloramphenicol and ampicillin, have been synthesized and revealed antibacterial action more strongly than parent drugs [16].

* **Corresponding author: Ayman H. Ahmed,** Chemistry Department, College of Science and Arts, Jouf University, Qurayat, Saudi Arabia; Chemistry Department, Faculty of Science, Al-Azhar University, Nasr City, Cairo, Egypt, e-mail: ahfahmi@ju.edu.sa

Leukemia is a cancer of the blood-forming tissue, which involves the lymphatic system and the bone marrow. In individuals with leukemia, abnormal white blood cells, which do not function properly, are produced by the bone marrow. Then, the healthy blood cells in the bone marrow are crowded by these abnormal cells, reducing the number of platelets, red blood cells and healthy white blood cells. The symptoms of this disease are weakness, chills, infection, enlarged liver and bleeding, bone pain and small red spots in the skin. Scientists do not comprehend the accurate reasons for leukemia. It seems to develop from a combination of environmental and genetic factors. Viable treatment techniques for human leukemia are being worked on, but so far none of them have been seen as totally acceptable. Nevertheless, the antileukemia activity of some metal–hydrazone complexes has been reported [17,18], the synthesized hydrazones and Mn(II) complexes were not yet researched. Therefore, we examined the synthesized compounds toward leukemia; in particular, the metal complexes have been recently demonstrated as less harmful and more potent in many cases in comparison with the free ligands.

In continuation of ongoing reports on some oxalic dihydrazones and their chelates [8–10], the present work portrays preparation, characterization and morphological investigations of divalent manganese complexes with two hydrazones as ligands. Antimicrobial and antileukemia activities of the manganese complexes and their corresponding ligands have been researched to show the plausibility of using them in pharmacology science.

2 Experimental

2.1 Materials and techniques

2-Hydroxynaphthalene-1-carbaldehyde, 2-methoxybenzaldehyde, manganese(II) acetate tetrahydrate and oxalic dihydrazide were acquired from Sigma-Aldrich. Solvents were utilized without any more refinement considering their highest purity. Elemental analyses, thermal (TG) and spectral (FT-IR, Mass, UV-Vis) measurements were carried out as published [9]. The ^{1}H-NMR spectra were obtained using a Varian mercury VX-300 NMR spectrometer at 300 MHz in DMSO-d_6. The chemical shifts were given in δ (ppm) and determined relative to tetramethylsilane (TMS). The ESR spectra of the complexes were recorded in the powder form at room temperature utilizing Bruker-EMX-(X-bands-9.7 GHZ) spectrometer at 100 kHZ frequency, microwave power 1.008 mW and modulation/amplitude of 4 GAUSS at National Center for Radiation Research and Technology, Egypt. By utilizing high vacuum technique, the solid complexes coated using gold sputter coater (SPI-Module, USA) were observed by scanning electron microscopy (model: JSM-5500 LV; JEOL Ltd, Japan). Employing Faraday's strategy, effective magnetic moments (μ_{eff}) at 4 Ampere for Mn(II) complexes were estimated at room temperature (RT).

2.2 Preparations

2.2.1 Isolation of ligands (BHO and BMO)

N,N′-Bis[2-hydroxynaphthylidene]amino]oxamide (BHO) and *N,N′*-bis[2-methoxybenzylidene]amino]oxamide (BMO) were prepared by the method published in ref. [9]. Oxalic dihydrazide (0.01 mol, 1.181 g) was dissolved in 40 mL distilled water by heating on a hot plate, and 30 mL of absolute ethanol was added. This hot solution of oxalic dihydrazide was mixed with the hot absolute ethanolic solution of the chosen aldehydes (keeping the molar proportion at 1 hydrazide:2 aldehyde). Precipitation of hydrazone was observed during the increment of aldehyde solution. The reaction mixture was heated under reflux for 3 h. The resulting precipitate was filtered while hot, and abundance of dihydrazide was avoided by washing with hot water. The excess of aldehyde was removed by absolute ethanol, and the ligand was dried at 80°C for 2 h in an electric oven (m.p. of two ligands >300). The chemical formula and molecular structure of the resulting hydrazones were determined by the elemental analyses (Table 1) and spectral (^{1}H-NMR and IR) data. Furthermore, mass spectra of BHO and BMO (Figure 1) showed M^+ (molecular ion peak) at *m/z* (found/calculated) = 327.1/426.4 and 355.0/354.4, respectively, which coincide well with the assumed formula. Schemes 1 and 2 provide mass fragmentation pathways of the investigated ligands.

2.2.2 Isolation of complexes

Manganese(II) complexes were formed via the interaction between divalent manganese acetate and the ligand as follows. First, the free hydrazone (0.56 mmol, 0.2 g) was dissolved in 35 mL hot DMF, and then, methanol (40 mL) was added. Then, 25 mL methanolic solution of metal acetate was gradually added to the previous ligand solution in 1 L:2 M molar proportion. The subsequent

Table 1: Analytical and physical data of the ligands and their related Mn(II) complexes

Compound (mol. wt.)	Symbol	Color	Yield (%)	Found (calcd) (%)			
				C	H	N	M
$C_{24}H_{18}N_4O_4$ 426.13	BHO	Yellow	98	68.30 (67.60)	5.11 (4.25)	12.84 (13.14)	—
$C_{18}H_{18}N_4O_4$ 354.36	BMO	White	78	59.49 (61.01)	5.60 (5.12)	15.47 (15.81)	—
$[Mn_2(BHO\text{-}H)_2(H_2O)_4]\cdot H_2O$ 1060.78	Mn–BHO	Brown	76	54.19 (55.48)	4.10 (3.99)	10.38 (10.56)	10.52 (10.36)
$[Mn(BAO\text{-}2H)(OAc)_2(DMF)_2]$ 671.56	Mn–BMO	Yellowish	25	49.39 (50.08)	5.60 (5.40)	12.28 (12.51)	9.10 (8.18)

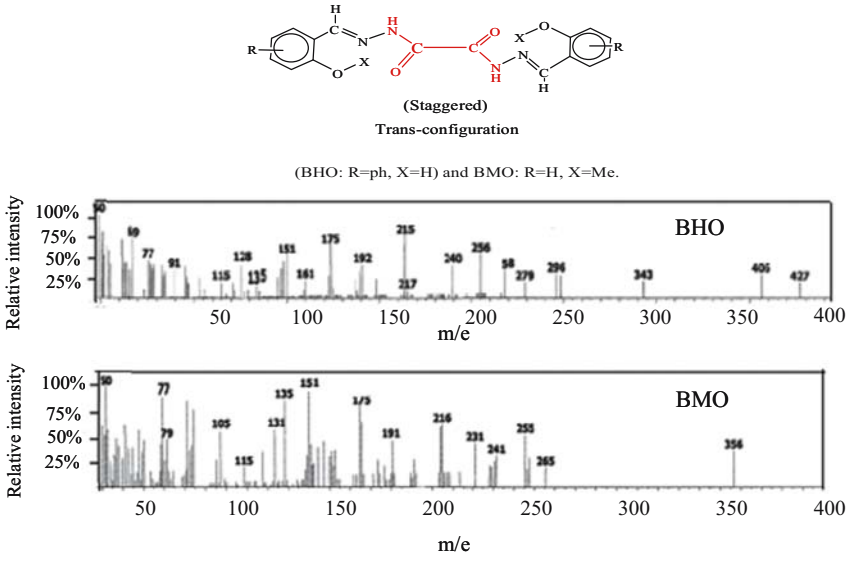

Figure 1: Mass spectra of the ligands (BHO and BMO).

mixture was refluxed for 3 h and then sifted on hot. The precipitate was washed using methanol and left overnight. To expel any trace of DMF solvent, the complex was washed thoroughly with methyl alcohol and propanone separately and finally dried at 80°C in an oven for 4 h (m.p. of two manganese(II) complexes >300).

2.3 Pharmacological screening

2.3.1 Antimicrobial activity

The susceptibility tests were performed by NCCLS proposals (National Committee for Clinical Lab Standards, 1993). The assessment of the restraint zone was done by the well diffusion strategy [19]. The inoculum obtained from the colonies grown overnight on an agar plate was inoculated into Mueller–Hinton broth. A sterile swab was immersed in the broth and inoculated on Mueller–Hinton agar plates. The samples were dissolved in DMSO at various concentrations (2.5, 5 and 10 mg/mL). The inhibition zone was estimated at 37°C after 24 h. Controls were obtained using DMSO.

2.3.2 Cytotoxic activity on leukemia cell lines

2.3.2.1 Chemical substances

Trypan blue dye, crystal violet and DMSO solvent were purchased from Sigma (USA). One percentage of crystal violet stain was made of 50% methanol: 0.5% crystal violet (w/v) was then made up to volume with bi-distilled H_2O and sifted through a filter paper (Whatman No. 1). RPMI-1640, Dulbecco's modified Eagle's medium (DMEM), gentamycin, L-glutamine, 0.25% trypsin–EDTA, HEPES buffer solution and fetal bovine serum were obtained from Lonza.

2.3.2.2 Cell culture

Mouse myelogenous leukemia cell line (M-NFS-60 cells) was acquired from VACSERA Tissue Culture Unit. Leukemia cells were maintained in the DMEM medium supplemented with 1% L-glutamine, HEPES buffer, 10% heat-inactivated fetal bovine serum and 50 µg/mL gentamycin at 37°C (humidified atmosphere) with 5% CO_2 two times a week.

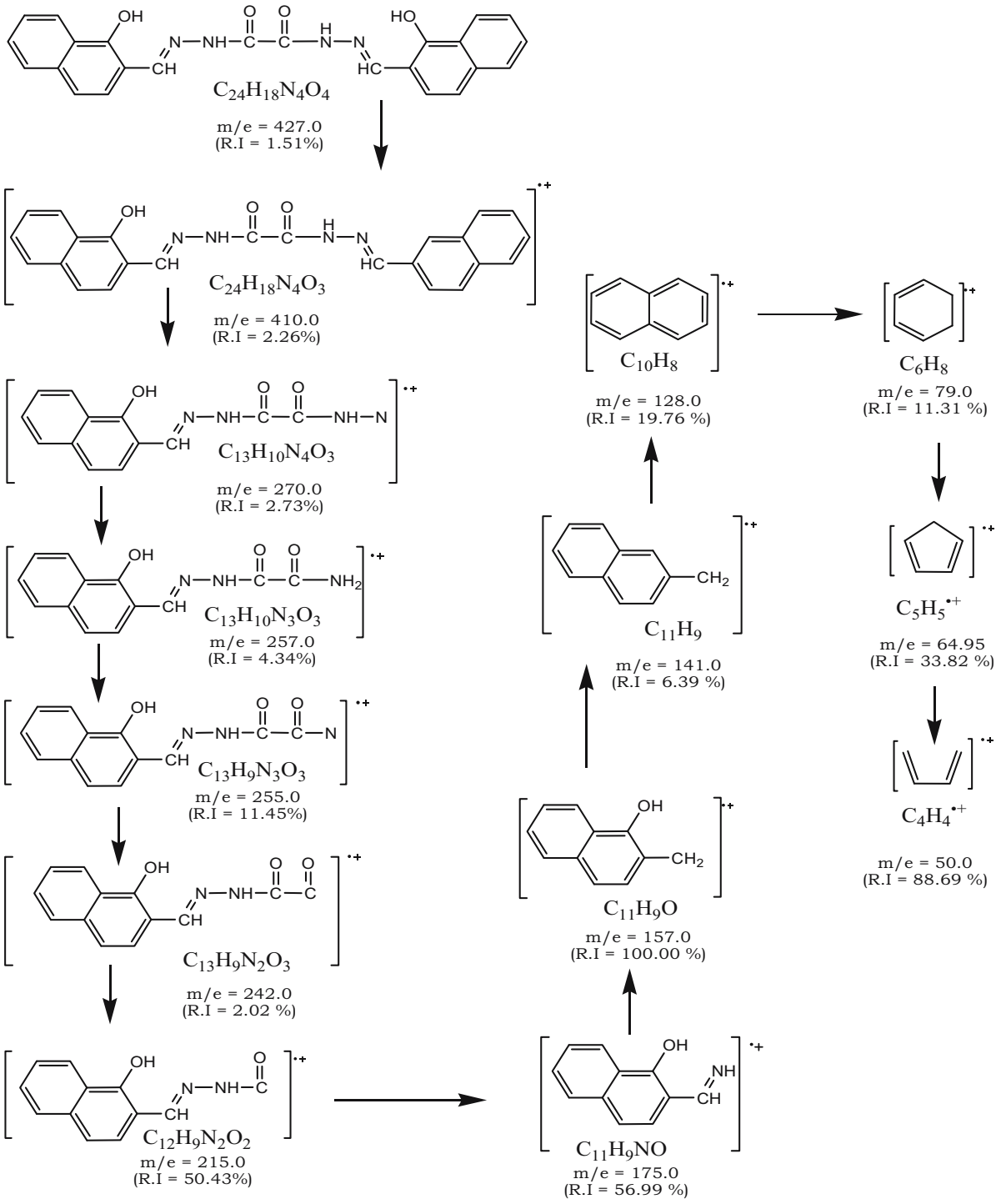

Scheme 1: Mass fragmentation of *N,N′*-bis[2-hydroxynaphthylidene]amino]oxamide (BHO).

2.3.2.3 Cytotoxicity assessment

In a 96-well plate containing 100 µL of growth medium, concentration of 1×10^4 cells was seeded. After 24 h of seeding, new fresh medium with different concentrations of the sample was added. Serial twofold dilutions of the examined ligand/complex were added to confluent cell monolayers distributed into flat-bottomed microtiter plates (96 wells). The microtiter plates incubated at 37°C for 24 h in a humidified incubator containing 5% CO_2. Without sample and with or without DMSO, the control cells were incubated. It was found that the examination was not influenced up to 0.1%

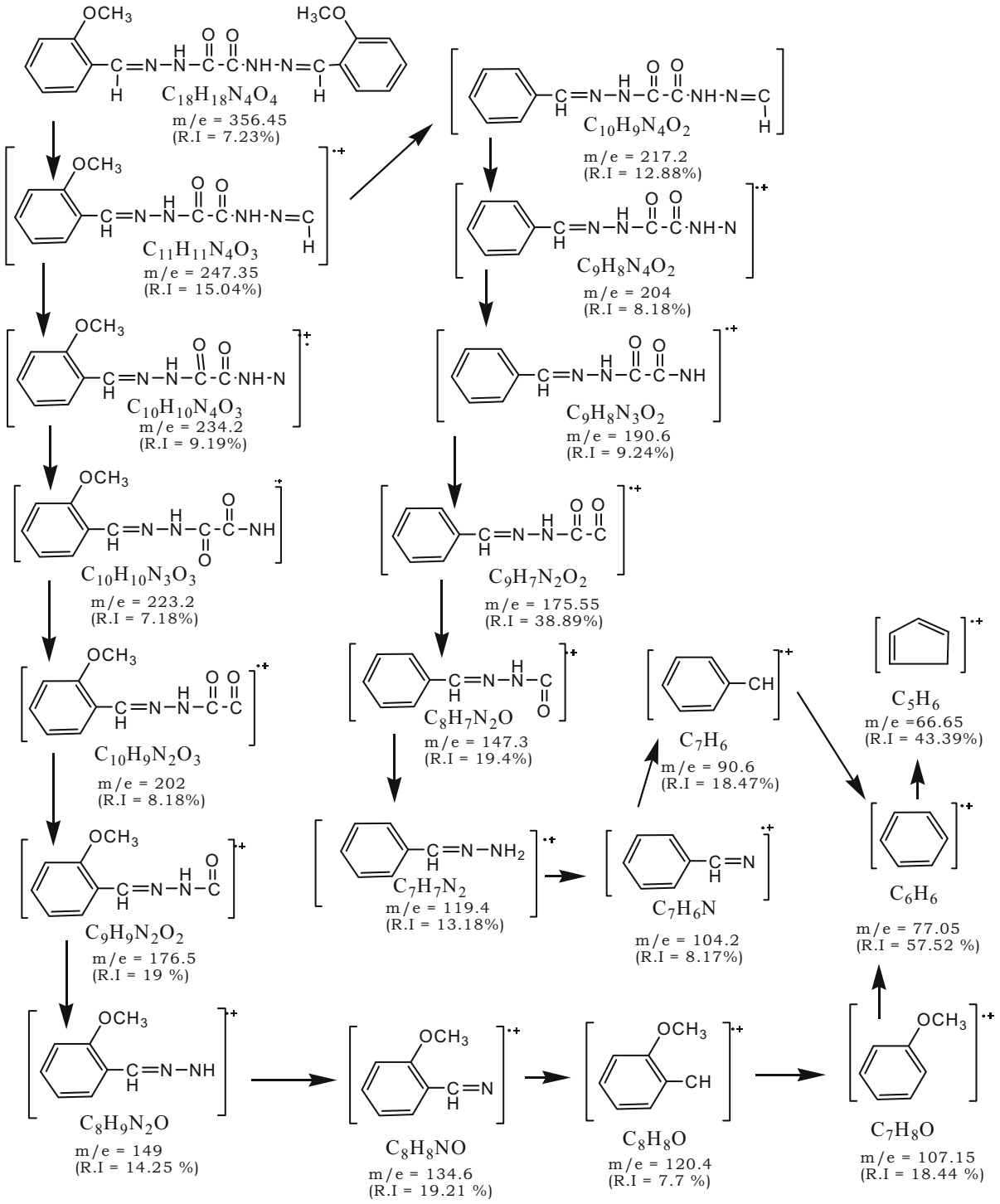

Scheme 2: Mass fragmentation of *N*,*N*′-bis[2-methoxybenzylidene]amino]oxamide (BMO).

of DMSO in the wells. After 24 h of incubation, the viable cell yield was estimated using a colorimetric method.

After the incubation period, the media were allowed to aspirate and 1% crystal violet solution was added to each plate and kept for 1/2 h. The stain was eliminated, and the microplates were washed by tap water. All wells were mixed thoroughly with 30% CH_3COOH, and the absorbance of the microplates (at λ = 490 nm) was measured. The optical density was estimated in a reader plate (Sun Rise, TECAN, Inc., USA), and the viability percentage was calculated according to the following equation:

$$\text{Viability percentage} = [1 - (\text{ODt}/\text{ODc})] \times 100\%$$

where ODt and ODc are the mean optical densities of wells treated and untreated with ligands/complexes, respectively.

The relationship between the ligand/complex concentration and the alive cells is graphically plotted, and IC_{50} was determined by Graph pad Prism program (San Diego, CA, USA) [20,21].

Ethical approval: The conducted research is not related to either human or animal use.

3 Results and discussion

Analytical and physical results of hydrazones ligands (BHO and BMO) and their related Mn(II) complexes (Mn–BHO and Mn–BMO) are summarized in Table 1.

3.1 IR spectroscopy

FT-IR spectral investigation of hydrazones and their manganese(II) complexes demonstrates the coordination behavior of the ligands within the chelation process.

Configuration of chosen ligands were discussed elsewhere [9] and alluded to the existence of keto forms, Figure 1 [22]. The two ligands were validated on the premise: BHO showed bands for $\nu OH_{naphthoic}$ (3,476 cm^{-1}), νNH (3,166 cm^{-1}), νC═O (1,705 cm^{-1} + 1,660 cm^{-1}), νC═N (1,621 cm^{-1}) and $\nu C{-}O_{naphthoic}$ (1,287 cm^{-1}). Meanwhile, BMO uncovered νC═O (1,653 cm^{-1}), νNH (3,202 cm^{-1}), νC═N (1,600 cm^{-1}), νOH_{enolic} (3,227 cm^{-1}) and νC–OMe (964 cm^{-1}) [23].

The infrared spectra of the Mn(II) complexes were examined and contrasted with those of related ligands. The method of chelation and structures was assured by the following actualities: for Mn–BHO: (1) the obscure of ν(NH) with noticeable of $\nu(C{=}O)_{complex}$ at 1,655 cm^{-1} provides an indisputable proof to the coordination of metal ion with the deprotonated NH group. (2) Also, the positive shift for $\nu(C{-}O)_{naphthoic}$ vibration (L : 1,287 → complex: 1,299 cm^{-1}) gives some insight to deprotonation of both naphthoic (OH) groups during their coordination, however remarking $\nu(OH)_{naphthoic}$ at lower value (3,186 cm^{-1}) points to the existence of naphthoic (OH) in H-bonding. (3) Splitting of the azomethine band in free ligand with its shift (ligand: 1,621 cm^{-1}: complex: 1,600, 1,618 cm^{-1}) justifies the sharing of this group in coordination where two dissimilar azomethine groups are formed (Figure 5) [24,25]. This supposition is boosted from the perception of $\nu(OH)_{naphthoic}$ and $\nu(OH)_{enolic}$ at 3,186 and 3,342 cm^{-1}, respectively. The lower offset associated with $\nu(OH)_{naphthoic}$ demonstrated the presence of H-bonding between the azomethine nitrogen and naphthoic OH groups. (4) Existence of a broad band in the complex at 3,379 cm^{-1} shows the overlapped crystalline/coordinated water molecules. In case of Mn–BMO, (1) the perception of C═O groups in the IR spectrum of Mn–BMO with obscure of ν(NH) band demonstrates that the BMO ligand favored its keto form in the chelation process. (2) Variation of ν(C═O) feature from strong (in ligand) to very strong (in complex) comparative with other neighbor bands indicates input of this group in coordination. (3) Undoubtedly, nonappearance of $\nu(M{-}O_{methoxy})$ with remaining NH, C═N and C–OMe groups at similar positions ruled out contribution of the previously mentioned groups in coordination. (4) The two bands related to ν_{as} and ν_s (carboxylic) of acetate group were seen at 1,351 cm^{-1} and 1,437 cm^{-1}, respectively. The larger difference between their locations affirmed the coordination of acetate as a unidentate anion through the C–O moiety of the carboxylic group [26]. (5) Furthermore, appearance of a new band at 1,729 cm^{-1} assignable to $\nu(C{=}O)_{DMF}$ affirmed the contribution of DMF solvent in coordination [27]. Surely, the presence of new $\nu(M{-}O_{naphthoic})$ and $\nu(M{-}O_{methoxy})$ in Mn–BHO and Mn–BMO spectra at 567 and 640 cm^{-1}, respectively, shows the formation of Mn–L bond.

3.2 ^{1}H-NMR spectroscopy

The NMR spectra of the ligands showed signals at various positions: in BHO ligand: 6.5–8.5 (aromatic protons, m), 9.7 (CH═N, s), 12.6 (OH, s), 12.8 (NH, s); in BMO: 3.93 (OCH_3, s), 6.8–8.5 (aromatic protons, m), 8.9 (CH═N, s), 11.9 (OH, s), 12.3 (NH, s). Vanishing of –OH and –NH protons upon supplying of D_2O affirmed the right assignment of these groups in the ligand spectrum. The two ligands are in harmony with staggered or syn-cis-conformation as the δCH═N, δNH and δOH resonances, each showed up as a singlet [28]. But which conformation is true? In fact, IR data information responded to this inquiry and guaranteed the staggered configuration [10].

3.3 Optical and magnetic investigations

The absorption bands of the ligands and their complexes in Nujol mull were assigned (Figure 2 and Table 2). In addition to the ligand bands, manganese complexes demonstrated d–d transitions from which the proposed geometry was predicted. The electronic information of manganese complexes was interpreted considering the two manganese(II)

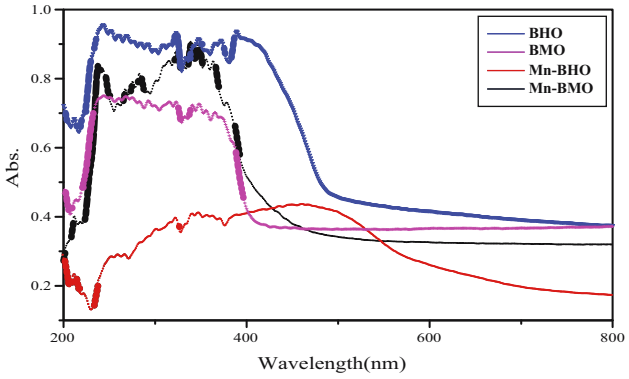

Figure 2: UV-Vis spectrum of free ligands and manganese(II) complexes in Nujol mull.

complexes have octahedral structures [29]. The bands ascribed to $^6A_{1g}$ (S) → $^4T_{1g}$, ^4E_g(G); $^4T_{2g}$, ^4E_g(D) and $^4T_{1g}$(P) transitions in manganese complexes are presumed to be overlapped/masked by strong peaks of free ligands.

The values of μ_{eff} in case of Mn–BHO and Mn–BMO complexes (Table 1) could be reliable with the proposed octahedral geometry [30]. A significant difference between the observed effective magnetic moment (6.2, Table 1) and the pure spin (5.95) in case of Mn–BHO can be elucidated as follows: high spin Mn–BHO complex is expected to have $\mu >$ 5.95 considering the presence of five single electrons in the two manganese ions of $[Mn_2(BHO\text{-}H)_2(H_2O)_4]\cdot H_2O$ complex. Spin of these single electrons in the same direction (Mn↑↑↑↑↑–↑↑↑↑↑Mn) gives very high magnetic moment. In reality, the obtained magnetization is not high since nearness of 2Mn ions near one another in the suggested configuration may cause spin coupling (partial quenching of the spin moments) that minimizes the magnetism. Magnetic data indicated the presence of five unpaired d electrons in both manganese(II) complexes ($t_{2g}^3 \cdot e_g^2$) affirming a paramagnetic nature.

3.4 Thermogravimetric investigation

Thermal disintegration examination of the synthesized consequential solid complexes has been performed, which reveals the thermal stability as well as the type and number of solvent molecules in the proposed configuration (Table 2). The TG thermograms of the two manganese complexes are shown in Figure 3. The Mn–BHO and Mn–BMO complexes exhibited five and four steps of degradation, respectively, concerning the gradual disintegration of metal complexes with consistence of metallic residue at final stage. TG curves illustrated that Mn–BHO and Mn–BMO begin to decompose at 300°C and 195°C, respectively, signifying that the Mn–BHO is more stable than Mn–BMO (Figure 3).

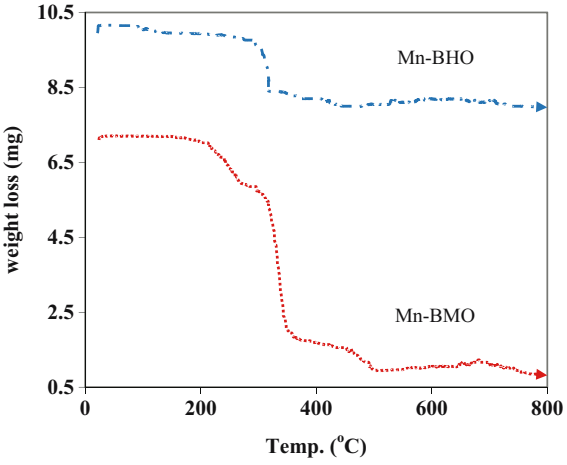

Figure 3: TG spectrum of manganese(II) complexes.

Table 2: Electronic spectral, magnetic moment and thermal data of ligands/Mn(II) complexes

Sample	Band position (nm)	Assignment	Configuration	$\mu_{eff.}$ (B.M.)	Temp. (°C)	TG Assignments	Found/ calcd (%)
BHO/BMO	380–420	n → π*(C=N)	—	—	—	—	—
	360–380	n → π*(C=O)					
	330–360	π → π*(C=N)					
	300–330	π → π*(C=O)					
	230–270	π → π*(Phenyl)					
Mn–BHO	590	$^6A_{1g}$(S) → $^4T_{1g}$(G)	Octahedral, D_{6h}	6.2	45–150	$H_2O_{crystalline}$	2.0/1.7
		$^6A_{1g}$(S) → $^4T_{2g}$(G)					
	480				178–310	$4H_2O_{coordinated}$	6.9/6.8
					620–800	Formation of 4(MnO + $MnCO_3$) mix.	70.8/71.0
Mn–BMO	420	$^6A_{1g}$(S) → $^4T_{1g}$(G)	Octahedral, D_{6h}	5.12	190–280	$2OAc_{coordinated}$	18.0/17.4
	378	$^6A_{1g}$(S) → $^4T_{2g}$(G)			590–800	Formation of MnO	11.1/10.6

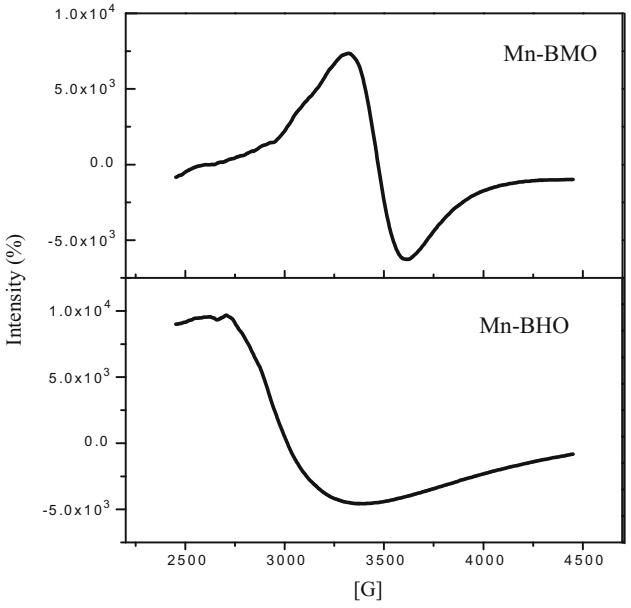

Figure 4: EPR spectra of solid manganese(II) complexes

3.5 Electron paramagnetic resonance (EPR)

The Mn–BHO and Mn–BMO solids have been analyzed by EPR spectroscopy at room temperature, and their spectra are shown in Figure 4. The ground state of the octahedral d^5 ion (spin free) is ^6A. The energy levels are at ±5/2, ±3/2 and ±1/2, and a single isotropic resonance at $g = 2$ is easily attained. Accordingly, the EPR spectra of manganese complexes display one wide signal for every complex with two "g" values (Mn–BHO: $g_{\|} = 1.88$ and $g_{\perp} = 1.93$ and Mn–BMO: $g_{\|} = 1.85$, $g_{\perp} = 1{,}998$). The nonappearance of hyperfine splitting for these complexes excluded any axial distortion. The average g values were calculated using the relation:

$$g_{av} = \frac{1}{3[g_{\|} + 2g_{\perp}]}$$

Both Mn–BHO and Mn–BMO revealed similar calculated g_{av} (1.9). The likeness in the ESR spectra and g values demonstrate that Mn–BHO and Mn–BMO take similar arrangements, i.e., octahedral geometry.

The average g value for both complexes (1.9) is almost near to free electron g value noting that the spin–orbit coupling is missing. The Mn–BHO ($g_{\|} = 1.88$) and Mn–BMO ($g_{\|} = 1.85$) complexes displayed $g_{\|}$ below 2.3, proposing the covalent nature of Mn–L bond, where the ionic M–L bond is characterized by $g_{\|} > 2.3$ [31,32]. Genuinely the nitrogen and oxygen coordination in manganese complexes is in congruence with high estimations of g [33].

In the light of the prior outcomes, the manganese complexes are anticipated to have structures presented in Figure 5.

3.6 Examining electron magnifying instrument (SEM)

The SEM micrographs of Mn(II)–BHO and Mn–BMO complexes are shown in Figure 6a, b and Table 3. It is shown in the figures that the Mn–BHO complex shows a platelet-like structure, while Mn–BMO complex displays a rod-like

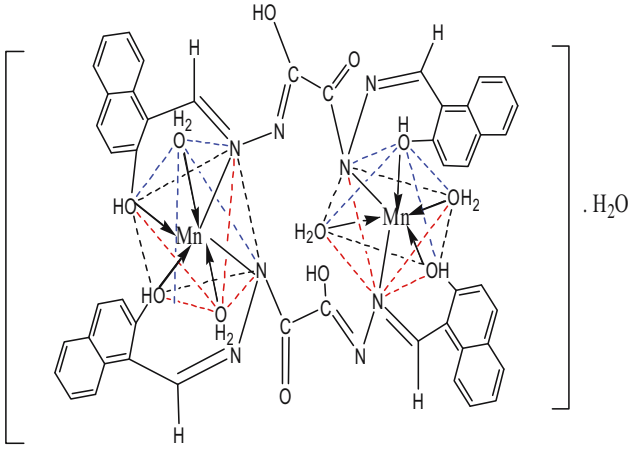

Mn-BHO

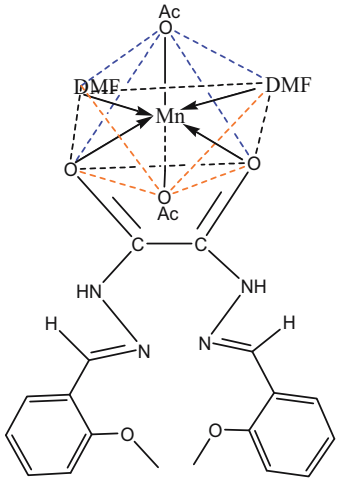

Mn-BMO

Figure 5: Suggested structures of manganese(II) complexes.

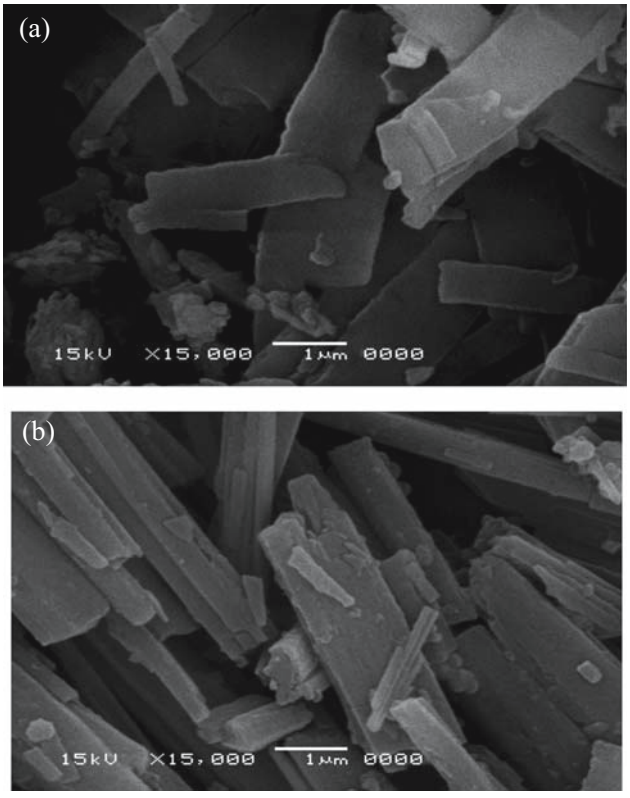

Figure 6: SEM micrographs of manganese(II) complexes (a) Mn-BHO; (b) Mn-BMO.

morphology. Isolation of two complex structures (Figure 5) is promoted from the acquisition of two SEM pictures with different morphologies (Figure 6). Clusters of larger size result from the aggregation of particles less than 100 nm in size. Average particle size of the two manganese complexes (2.5–14.5 µm) is in the diameter scope of few microns (Table 3).

3.7 Pharmacological significance

3.7.1 Antibacterial investigations

Antibacterial activities of ligands (BHO and BMO) and their complexes against gram-negative (*Proteus*, *Escherichia coli*) and gram-positive (*Bacillus subtilis*, *Staphylococcus aureus*) bacteria are shown in Figure 7. Free ligands showed lower activity in comparison to manganese complexes toward all the tested strains. The higher action of complexes can be illustrated in terms of chelation hypothesis [34]. On coordination, the polarity of the manganese(II) ion will be diminished to a more prominent degree because of the interaction between the ligand orbitals belong to donor groups and the positive charge of the metal. Furthermore, the complexation process will induce the delocalization of p-electrons over the chelating ring and enhances the penetration of the complex into lipid membranes and blocking of the metal binding sites in the enzymes of bacteria. In addition, the metal complex influences the breath process of the cell and hence obstructs the synthesis of proteins restricting further growth of the organisms [35]. The additional factors that enhance the action are Mn–L bond length and solubility [36].

3.7.2 Cytotoxic impact

Hydrazones ligands and their manganese complexes were screened against mouse myelogenous leukemia (M-NFS-60) carcinoma cells under the test conditions. The cell viability values are shown in Figure 8. Table 3 presents the concentrations of the examined samples that restrain half of cell multiplication (IC_{50}), in which the parent compounds were less cytotoxic than their complexes. In the literature, cytotoxic activity increases upon complexation, and *vice versa* [37,38]. In this study, coordination appeared to be a good strategy. In our data, the cytotoxic activity of hydrazones was improved upon chelation with manganese(II) ions, resulting in complexes with noteworthy cytotoxicity against M-NFS-60. This can be interpreted on the premise the manganese tie to two DNA sites of cancer cells subsequent to releasing $2H_2O$ molecules in case of Mn–BHO and two DMF and/or OAc in case of Mn–BMO [337] (Figure 5).

Table 3: SEM results and inhibition of M-NFS-60 cell line by ligands and their Mn(II) complexes

Compound	IC_{50} (µg/mL)	Concentration at which inhibition begins (µg/mL)	SEM			Morphology
			Particle size (µm)			
			Max.	Min.	Av.	
BHO	92.1 ± 4.5	5.9	—	—	—	
BMO	408 ± 9.8	62.5	—	—	—	
Mn–BHO	58.7 ± 2.7	4.2	5.0	0.066	2.5	Platelet
Mn–BMO	183 ± 6.1	15.6	28.5	0.057	14.5	Rod

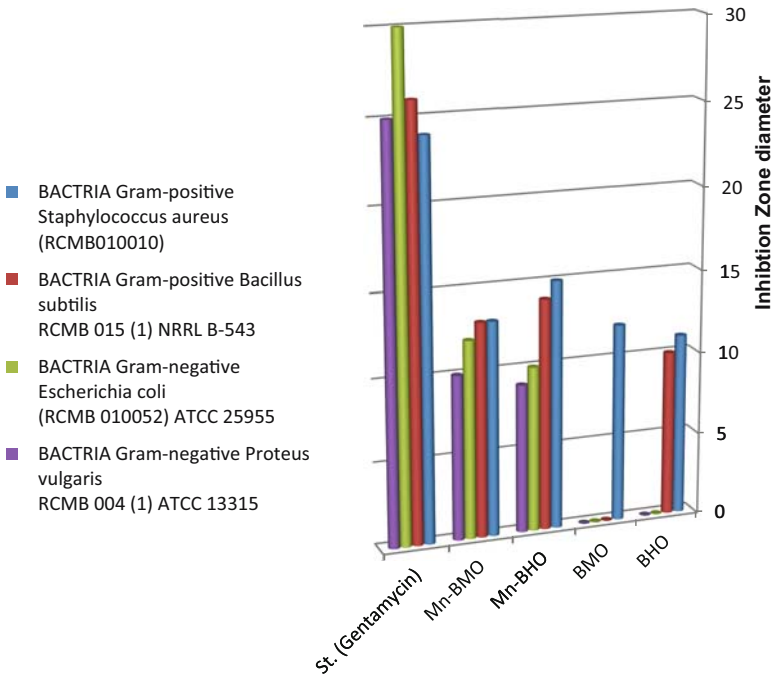

Figure 7: Antibacterial activity for ligands and their manganese(II) complexes.

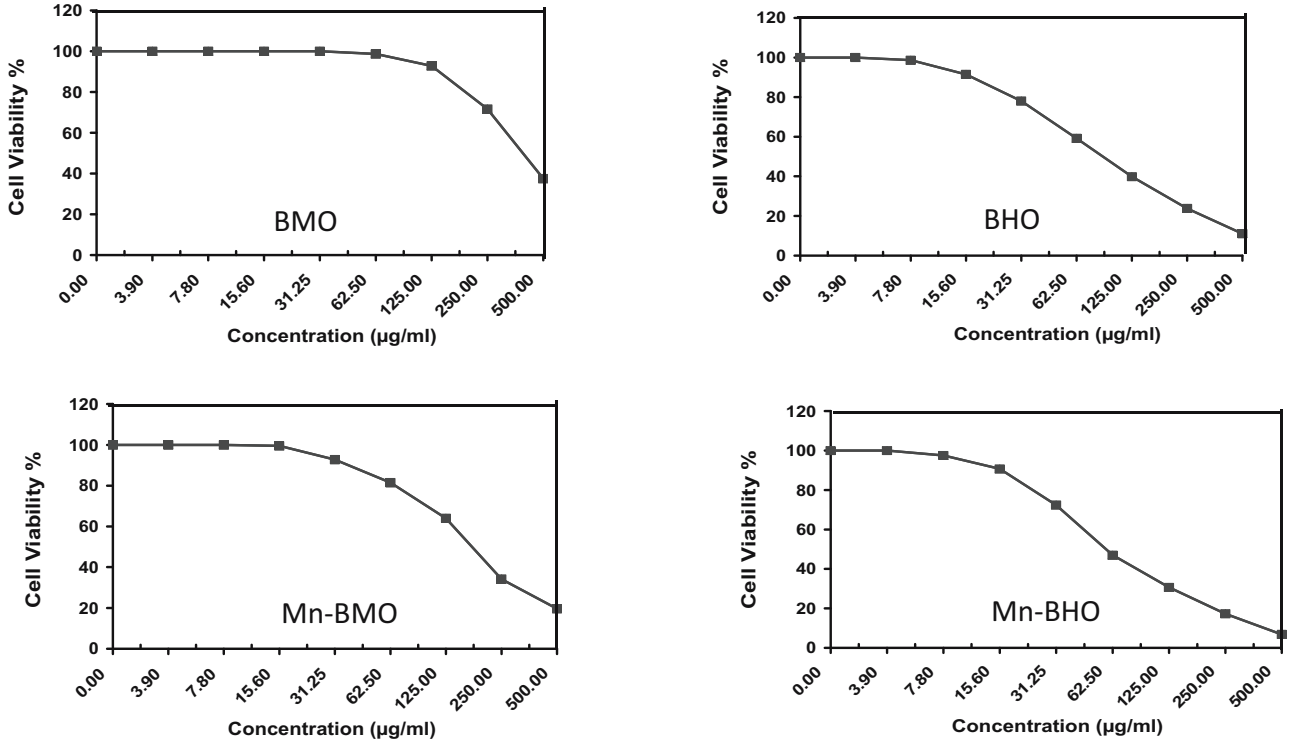

Figure 8: Cytotoxicity evaluation of ligands and their manganese(II) complexes against M-NFS-60 cell line.

The oxalic dihydrazones and their Mn(II) complexes begin to inhibit the M-NFS-60 cell line proliferation at concentrations listed in Table 3. Among the examined compounds, inhibitory impact against the M-NFS-60 cells was changed by the order Mn–BHO > BHO > Mn–BMO > BMO.

4 Conclusion

Hydrazones and their Mn(II)-complexes can be isolated in a pure form. The conventional reflux strategy might be utilized for this purpose. Contrasting of theoretical and experimental percentages of elemental analyses demonstrates that the proposed formulae agree well with the chemical compositions of the isolated compounds. Consistence of the coveted complexes can be affirmed from the UV-Vis, FT-IR, ESR and magnetic data. Monitoring the color change of the ligand during the complexation process can be considered as further evidence for the formation of required complexes. Both Mn(II)–bis[2-hydroxynaphthylidene]amino]oxamide and Mn(II)–bis[2-methoxybenzylidene]amino]oxamide complexes have octahedral configurations. With the antibacterial action against four microorganisms, the outcomes suggested that the complexes are increasingly powerful and might impede protein creation of certain microorganisms. In addition, the antileukemia impact of the free hydrazones was enhanced by coordination. The Mn(II)–bis[2-hydroxynaphthylidene]amino]oxamide chelate displayed a significant cytotoxic activity against mouse myelogenous leukemia carcinoma cells compared with other examined compounds.

Conflict of interest: Author states no conflict of interest.

References

[1] Mohan M, Gupta NS, Gupta MP, Kurnar A, Kurnar M, Jha NK. Acta, Synthesis, characterization and antitumor activity of some metal complexes of 3- and 5-substituted salicylaldehyde o-hydroxybenzoylhydrazones. Inorg Chim. 1988;152:25–36.

[2] Barbazan P, Carballo R, Covelo B, Lodeiro C, Lima JC, Vazquez-Lopez EM. Synthesis, characterization, and photophysical properties of 2-hydroxybenzaldehyde [(1*E*)-1-pyridin-2-ylethylidene]hydrazone and its rhenium(I) complexes. Eur J Inorg Chem. 2008;2713–20.

[3] Hollingshaus JG. Inhibition of mitochondrial electron transport by hydramethylnon: a new amidinohydrazone insecticide. Pestic Biochem Physiol. 1987;27:61–70.

[4] Sherif EM, Ahmed AH. Synthesizing new hydrazone derivatives and studying their effects on the inhibition of copper corrosion in sodium chloride solutions. Synth React Inorg Met-Org Chem. 2010;40:365–72.

[5] Singh VP, Katiyar A. Synthesis, structural characterization and antimicrobial activity of some transition metal(II) complexes with acetone p-amino acetophenone benzoylhydrazone. Pestic Biochem Phys. 2008;92:8–14.

[6] Singh VP, Singh P, Singh AK. Synthesis, structural and corrosion inhibition studies on cobalt(II), nickel(II), copper(II) and zinc(II) complexes with 2-acetylthiophene benzoylhydrazone. Inorg Chim Acta. 2011;379:56–63.

[7] Syiemlieh I, Kumar A, Sunshine DK, Lal RA. Synthesis, characterization and structure assessment of mononuclear and binuclear low-spin manganese(II) complexes derived from oxaloyldihydrazones, 1,10-phenanthroline and 2,2′-bipyridine. J Mol Struct. 2018;1166:252–61.

[8] Ahmed AH, Hassan AM, Gumaa HA, Mohamed BH, Eraky AM. Nickel(II)-oxaloyldihydrazone complexes: characterization, indirect band gap energy and antimicrobial evaluation. Cogent Chem. 2016;2:1142820.

[9] Ahmed AH, Hassan AM, Gumaa HA, Mohamed BH, Eraky AM, Omran AA. Copper(II)-oxaloyldihydrazone complexes: physico-chemical studies; energy band gap and inhibition evaluation of free oxaloyldihydrazones toward the corrosion of copper metal in acidic medium. Arabian J. Chem. 2019;12:4287–302.

[10] Ahmed AH, Hassan AM, Gumaa HA, Mohamed BH, Eraky AM. Physicochemical studies on some selected oxaloyldihydrazones and their novel palladium(II) complexes along with using oxaloyldihydrazones as corrosion resistants. Inorg Nano-Metal Chem. 2017;47(12):1652–63.

[11] Abd El-Wahab H, Abd El-Fattah M, Ahmed AH, Elhenawy AA, Alian NA. Synthesis and characterization of some arylhydrazone ligand and its metal complexes and their potential application as flame retardant and antimicrobial additives in polyurethane for surface coating. J Organomet Chem. 2015;791:99–106.

[12] Bekheit MM, El-Shobaky AR, Gad Allah MT. Synthesis, spectroscopic characterization and antimicrobial studies of some metal complexes with 2-acetylpyridine phenoxyacetyl hydrazone (HAPPA). Arab J Chem. 2017;10:S3064–72.

[13] Desoky A, Mohamad M, Abualreish MJA, Abu-Dief AM. Antimicrobial and anticancer activities of cobalt (III)-hydrazone complexes: solubilities and chemical potentials of transfer in different organic co-solvent-water mixtures. J Mol Liq. 2019;290:1–10.

[14] Savanini L, Chiasserini L, Gaeta A, Pellerano C. Synthesis and anti-tubercular evaluation of 4-quinolylhydrazones. Biorg Med Chem. 2002;10:2193–8.

[15] Ghasemian M, Kakanejadifard A, Azarbani F, Zabardasti A, Shirali S, Saki Z, et al. The triazine-based azo-azomethine dyes; synthesis, characterization, spectroscopy, solvatochromism and biological properties of 2,2′-(((6-methoxy-1,3,5-triazine-2,4-diyl)bis(sulfanediyl)bis(2,1-phenylene))bis(azanylylidene)bis(methanylylidene))bis(4-(phenyldiazenyl) phenol). Spectrochim Acta A. 2015;38:643–7.

[16] Ajani O. Synthesis, characterization, antimicrobial activity and toxicology study of some metal complexes of mixed antibiotics. Afr J Pure Appl Chem. 2008;2(7):69–74.

[17] Ferraz KSO, Ferandes L, Carrilho D, Pinto MCX, Leite MF, Souza–Fagundesb EM, et al. 2-Benzoylpyridine-N(4)-tolyl thiosemicarbazones and their palladium(II) complexes: cytotoxicity against leukemia cells. Bioorg Med Chem. 2009;17:7138–44.

[18] Pahontu E, Julea F, Rosu T, Purcarea V, Chumakov Y, Petrenco P, et al. Antibacterial, antifungal and in vitro antileukaemia activity of metal complexes with thiosemicarbazones. J Cell Mol Med. 2015;19(4):865–78.

[19] Hindler JA, Howard BJ, Keiser JF. Antimicrobial agents and Susceptibility testing. In: Howard BJ, editor, Clinical and pathogenic microbiology. St. Louis, MO, USA: Mosby-Year Book Inc.; 1994.
[20] Mosmann T. Rapid colorimetric assay for cellular growth and survival: application to proliferation and cytotoxicity assays. J Immunol Methods. 1983;65:55–63.
[21] Gomha SM, Riyadh SM, Mahmmou EA, Elaasser MM. Synthesis and anticancer activities of thiazoles, 1,3-thiazines, and thiazolidine using chitosan-grafted-poly(vinylpyridine) as basic catalyst. Heterocycles. 2015;91(6):1227–43.
[22] Lal RA, Adhikari S, Kumar A. Spectroscopic studies of isomerization of coordinated dihydrazone in tetranuclear dioxouranium(VI) complexes derived from bis(o-hydroxy-naphthaldehyde)oxaloyldihydrazone. Indian J Chem. 1997;36:1063–7.
[23] Burger K, Ruff I, Ruff F. Some theoretical and practical problems in the use of organic reagents in chemical analysis – IV: infra-red and ultra-violet spectrophotometric study of the dimethylglyoxime complexes of transition metals. J Inorg Nucl Chem. 1965;27:179–90.
[24] Ali AM, Ahmed AH, Mohamed TA, Mohamed BH. Chelates and corrosion inhibition of newly synthesized schiff bases derived from o- tolidine. Transit Met Chem. 2007;32:461–7.
[25] Salapathy S, Sahoo B. Salicylaldazinate metal chelates and their I.R. spectra. J Inorg Nucl Chem. 1970;32:2223–7.
[26] Nakamoto K. Inorganic spectra of inorganic and coordination compounds. 2nd ed. New York: John Wiley & Sons; 1970.
[27] Kumar D, Syamal A, Sharma LK. Synthesis and characterization of polystyrene-anchored monobasic bidentate Schiff base and its complexes with bi-, tri-, tetra- and hexavalent metal ions. J Coord Chem. 2008;61:1788–96.
[28] Kumar A, Lal RA, Chanu OB, Borthakur R, Koch A, Lemtur A, et al. Synthesis and characterization of a binuclear copper(II) complex $[Cu(H_2slox)]_2$ from polyfunctional disalicylaldehyde oxaloyldihydrazone and its heterobinuclear copper(II) and molybdenum(VI) complexes. J Coord Chem. 2011;64:1729–42.
[29] Cotton FA, Wilkinson G. Advanced inorganic chemistry. 2nd ed. New York: Interscience Publishers; 1966.
[30] Lee JD. Consize inorganic chemistry. 5th ed. London: Blackwell Science Ltd; 1996. p. 669.
[31] Lal RA, Basumatary D, Adhikari S, Kumar A. Synthesis and properties of mononuclear and binuclear molybdenum complexes derived from bis(2-hydroxy-1-naphthaldehyde)oxaloyldihydrazone. Spectrochim Acta A. 2008;69:706–14.
[32] Liver ABP. Inorganic electronic spectroscopy. New York: Elsevier; 1984.
[33] Kivelson D, Nieman R. ESR Studies on the bonding in copper complexes. J Chem Phys 1961;35:149–55.
[34] Mishra L, Singh VK. Synthesis, structural and antifungal studies of Co(II), Ni(II), Cu(II) and Zn(II) complexes with new Schiff bases bearing benzimidazoles. Indian J Chem. 1993;32:446–9.
[35] Kavitha P, Reddy KL. Synthesis, spectral characterisation, morphology, biological activity and DNA cleavage studies of metal complexes with chromone schiff base. Arab J Chem. 2016;9:596–605.
[36] Chohan ZH, Iqbal MS, Aftab SK. Design, synthesis, characterization and antibacterial properties of copper(II) complexes with chromone derived compounds. Appl Organomet Chem. 2010;24:47–56.
[37] Quiroga AG, Pérez JM, Montero EI, Masaguer JR, Alonso C, Navarro-Ranninger C. Palladated and platinated complexes derived from phenylacetaldehyde thiosemicarbazone with cytotoxic activity in cis-DDP resistant tumor cells. Formation of DNA interstrand cross-links by these complexes. J Inorg Biochem. 1998;70:117–23.
[38] Reis DC, Pinto MCX, Souza-Fagundes EM, Rocha LF, Pereira VRA, Melo CML,et al. Investigation on the pharmacological profile of antimony(III) complexes with hydroxyquinoline derivatives: anti-trypanosomal activity and cytotoxicity against human leukemia cell lines. Biometals. 2011;24:595–601.